Eidgenössische Technische Hochschule Zürich

Ecole polytechnique fédérale de Zurich
Politecnico federale di Zurigo
Swiss Federal Institute of Technology Zurich

The Method of Transport for solving the Euler-equations

M. Fey

Research Report No. 95-15
December 1995

Seminar für Angewandte Mathematik
Eidgenössische Technische Hochschule
CH-8092 Zürich
Switzerland

The Method of Transport for solving the Euler-equations

M. Fey

Seminar für Angewandte Mathematik
Eidgenössische Technische Hochschule
CH-8092 Zürich
Switzerland

Research Report No. 95-15 December 1995

Abstract

In many technical applications it is necessary to compute a numerical solution of complex flow problems in several space dimensions. Most available codes split the multi-dimensional problem into several one-dimensional ones. Those are aligned with the cell interfaces of the underlying grid. In some of the applications, e.g. high Mach number flow, this approach does not work very well, since the physical properties of the model equations are not represented correctly.
In this paper a new idea to solve the multi-dimensional Euler equations numerically is presented. It is the aim of this paper to obtain a robust shock capturing method without the use of dimensional splitting and to get a better understanding of multi-dimensional phenomena. The starting point of this idea is the one-dimensional flux vector splitting and the homogeneity of the Euler equations. Using this concept it is shown that a different interpretation of the one-dimensional waves and the use of the characteristic surfaces lead to a decomposition of the state vector into three multi-dimensional waves. This idea includes the physical properties of the linearized Euler equations, i.e. it allows infinitely many propagation directions.
Numerical results are shown at the end of this paper. It turns out that in special test cases, the multi-dimensional approach shown here and the dimensional splitting approach lead to structural differences even in a first order calculation.

Keywords: conservation laws, flux vector splitting, characteristic surfaces

Subject Classification: 65M06, 76M25, 76N15

1 Introduction

In many technical applications there is a need to calculate difficult flow problems numerically. Examples are the simulation of sub-sonic flow in tubes, the computation of combustion processes in engines and turbines, the calculation of the flow around wings of airplanes or the computation of the reactive hypersonic-sonic flow past reentry vehicles. All these examples are described in a first approximation by the Euler equations. This mathematical model of the flow does not include viscous effects and has to be adapted to special problems (e.g. chemical reactions). Most of these engineering applications have complex geometries and are always multi-dimensional.

For one-dimensional problems, there exist a number of numerical methods which can be used to calculate the solution, e.g. TVD, ENO or artificial viscosity methods. There are also some theoretical results for the class of hyperbolic conservation laws that the Euler equation belongs to. This is related to the existence of an analytic solution for problems with special initial conditions, called Riemann problems (RP).

However, solution methods developed for the 1-D case cannot be adapted to the multi-dimensional case. One reason is that there is no simple solution for a two-dimensional RP. Schultz-Rinne in [24] classifies 2-D RP's under the assumption that only one wave, i.e. shock, contact surface or rarefaction wave, is allowed for each discontinuity. The complexity of such solutions and the sensitivity to the initial conditions show that it is hopeless to either find an analytic solution for arbitrary data or use these RP's to construct multi-dimensional methods.

The same problem arises for other approaches e.g. flux vector splitting or flux difference splitting. Here the reason is that the Euler equations have infinitely many propagation directions in 2-D.

In the last few years, attempts have been made to circumvent this dimensional splitting approach and to introduce a better description of the flow properties into the code. The schemes for multidimensional flow can be divided into three classes as done by Roe in [19]. The first class uses the dimensional splitting approach and is called one-dimensional. The second class, called 1.5-dimensional, contains schemes which still use 1-D Riemann solvers but in directions different from the coordinate directions. R. LeVeque has constructed a numerical scheme based on this idea. He uses Riemann solvers normal and tangential to the cell interface in one time step. Hence, influences of the cross derivatives can be determined, this is in contrast to the 1-D schemes [15],[16].

The last class includes "truly" multidimensional schemes. At present, two ideas have gained a certain popularity. One was introduced by Roe, Struijs and Deconick in [21], [23]. They propose a new set of variables, comparable to the Roe averages in one space dimension. In these variables the flux can be linearized at this average value. The residual, which is the divergence of the flux, can be calculated explicitly, when these variables are assumed linear in space. Using a cell vertex discretisation, it is straightforward to calculate the residual for each triple of nodes. The next step is to distribute the local residual to neighboring nodes, in order to advance the solution to the next time step. Different wave models are proposed by different authors to solve this problem [22], [13], [18]. However, like all multi-dimensional approaches, these are only approximations to a 2-D RP, for the reasons mentioned above.

Another idea was put forward by Hirsch and Deconick [13]. They try to diagonalize the Euler equation locally. However, the Jacobian matrices of the flux in x- and y-direction are not simultaneously diagonalizable. So they introduce two directions κ_1 and κ_2 to transform the Jacobians in a special form. For a special choice of κ_1 or κ_2, in most cases the pressure or velocity gradient, one of the Jacobians vanishes so that one obtains a one-dimensional problem which can be diagonalized. These directions are strongly dependent on the flow properties, which results in a loss of robustness of the scheme.

In this paper we propose another technique to describe multi-dimensional flow. There are two ideas involved. First, we introduce the idea of transport by means of a scalar advection equation. Second, we generalize and adopt this method to the system case. The resulting scheme includes an important physical property of the linearized Euler equations by allowing infinitely many propagation directions. We use characteristic theory to get a good description of the propagation, and finite volume and conservation techniques to capture discontinuities. A new interpretation is given to the flux vector splitting, which enables us to reformulate it into a numerical scheme for arbitrary many space dimensions.

In the first part of this paper we will describe some one-dimensional numerical schemes. The Godunov-method and the idea of flux-difference splitting is shown briefly. We will look more into the details of the flux-vector splitting method, since a modification and a new interpretation of this approach will lead to the new method. We will also show some of the problems of adapting these approaches to several space dimensions. Next, we introduce the idea of transport by means of the scalar advection equation. Here, the physical or characteristic propagation direction is used to calculate contributions from one cell to its neighboring cells. The standard dimensions splitting uses the grid induced coordinate directions to calculate the flux across cell boundaries.

In the last part of this paper, we will show the modifications necessary to use the idea of transport for the non-linear system of the compressible Euler equations. We will motivate these changes in a heuristic way. Next, we will define the notion of multi-dimensional waves and the concept of contributions in a mathematical formalism. Finally, we show how this formalism leads to the new numerical method. Some numerical test calculations are also presented.

2 The scalar case

In this section we will briefly describe the main idea of transport and its two underlying principles; finite volume discretisation and method of characteristics, as proposed in [11]. For this purpose, it is sufficient to look at the linear equation in conservation form. Without loss of generality, we can restrict ourselves to two space dimensions. The equation has the form

$$h_t + (a(x,y)\,h)_x + (b(x,y)\,h)_y = 0 \tag{1}$$

where h is the unknown solution and $a, b : I\!R^2 \to I\!R$ are given real functions.

The space is discretised with a cartesian mesh of step size Δx and Δy in the x- and y-direction, respectively. The center of the finite volume i, j is located at the nodes (x_i, y_j) at $x_i = i\,\Delta x$, $y_j = j\,\Delta y$ and the cell interface at $x_{i\pm1/2} = (i \pm 1/2)\,\Delta x$ and $y_{j\pm1/2} = (j \pm 1/2)\,\Delta y$. We use the average value of the function h over each cell as the dependent variable, i.e.

$$h^n_{i,j} = \frac{1}{|V_{i,j}|} \int\limits_{V_{i,j}} h(x, y, n\,\Delta t) dx\, dy, \tag{2}$$

with $V_{i,j} = [x_{i-1/2}, x_{i+1/2}] \times [y_{j-1/2}, y_{j+1/2}]$ the domain of cell i, j. $|V_{i,j}|$ denotes its volume. Integrating the conservation law (1) over space and time

$$\int\limits_t^{t+\Delta t} \int\limits_{V_{i,j}} h_t(x,y,t)\,dx\,dy\,dt + \int\limits_t^{t+\Delta t} \int\limits_{V_{i,j}} \operatorname{div}\left(h(x,y,t) \begin{pmatrix} a(x,y) \\ b(x,y) \end{pmatrix} \right) dx\,dy\,dt = 0$$

and using Gauss theorem and the definition in (2), we get

$$|V_{i,j}|\,(h^{n+1}_{i,j} - h^n_{i,j}) + \int\limits_t^{t+\Delta t} \int\limits_{\partial V_{i,j}} h(x,y,t) \begin{pmatrix} a(x,y) \\ b(x,y) \end{pmatrix} \mathbf{n}\, dO\, dt = 0,$$

where $\partial V_{i,j}$ is the surface of the domain $V_{i,j}$. Since the function h is not known for time larger than t, the second integral can only be computed approximately. The simplest choice is to keep h, a and b constant in each cell. With the notation

$$a_{i,j} = a(x_i, y_j), \qquad b_{i,j} = b(x_i, y_j)$$

and the assumption that $a, b > 0$, we obtain the following numerical method

$$|V_{i,j}| \left(h_{i,j}^{n+1} - h_{i,j}^{n}\right) + \Delta t \left(\Delta y \left(h_{i,j}^{n}\, a_{i,j} - h_{i-1,j}^{n}\, a_{i-1,j}\right) + \Delta x \left(h_{i,j}^{n}\, b_{i,j} - h_{i,j-1}^{n}\, b_{i,j-1}\right)\right) = 0. \tag{3}$$

in conservation form. In the special case of the linear equation (1), the functions a and b are known everywhere and can be evaluated at the cell interfaces. However, when solving a non-linear system of equations, the method (3) is more appropriate; in that case the velocities a and b are functions of the solution, which is only known at the cell center. Approach (3) introduces the cell normals into the numerical method as shown in Figure 1. This leads to a strong dependence of the numerical solution on the underlying grid. It is the aim of this paper to replace these fluxes in the normal direction by a procedure more related to the true 'physics' of the problem.

The theory of characteristics use a different property of (1) to advance the solution in time. Along the integral curves $(x(t), y(t))^T$ given by

$$\begin{pmatrix} \dot{x} \\ \dot{y} \end{pmatrix} = \begin{pmatrix} a(x,y) \\ b(x,y) \end{pmatrix} \quad \text{with} \quad \begin{pmatrix} x(0) \\ y(0) \end{pmatrix} = \begin{pmatrix} x_0 \\ y_0 \end{pmatrix}, \tag{4}$$

the solution $h(x(t), y(t), t)$ of (1) reduces to the ODE

$$\frac{d}{dt} h(x(t), y(t), t) = -h(x(t), y(t), t) \left(\frac{\partial}{\partial x} a(x(t), y(t)) + \frac{\partial}{\partial y} b(x(t), y(t))\right) \tag{5}$$

with initial conditions $h(x_0, y_0, 0) = h_0(x_0, y_0)$. Independent of the number of space dimensions, there is only one propagation direction for each point. Thus, in the scalar case this transformation always reduces the problem to the integration of an ODE. For the linear equation (1) and smooth functions a and b, (4) can always be integrated numerically and the solution of h at any time t can be computed in one step. This idea can also be generalized to non-linear scalar equations (see [2]). In the case of a non-linear system, the equations no longer reduce to an ODE, since the characteristics of different families interact. The treatment of occurring shocks is more difficult when using the method of characteristics.

The new approach combines both ideas: the finite volume formulation to capture shocks and the characteristic part to select the physical propagation directions. The characteristic curves (4) are used to trace the transport of quantities. Hence, the normal flux across a cell boundary is replaced by a transport from one domain to another domain, using the physical propagation directions (Figure 2).

We can describe this behavior analytically using Dirac's delta function. Let h^u be an approximation of $h(x, y, t + \Delta t)$ using (5) and let $\mathbf{u} = (\dot{x}, \dot{y})^T = (a, b)^T$. For small time steps Δt we can replace the integration in (4) by a simple Euler step and get

$$h^u(\mathbf{x}, t, \Delta t) = \int_{I\!R^N} h(\mathbf{y}, t) \delta(\mathbf{x} - (\mathbf{y} + \Delta t \mathbf{u}(\mathbf{y}))) d\mathbf{y} \tag{6}$$

up to first order. The δ-function "searches" backward for the point $\mathbf{y}$ that determines the value of h at $(\mathbf{x}, t + \Delta t)$. For simplicity, we drop the index i, j, since all actions are the same at each cell. We define $\Omega_0 = V_{i,j}$, the domain of the center cell, and Ω_i, $i = 1, ..., 8$, the neighboring cells

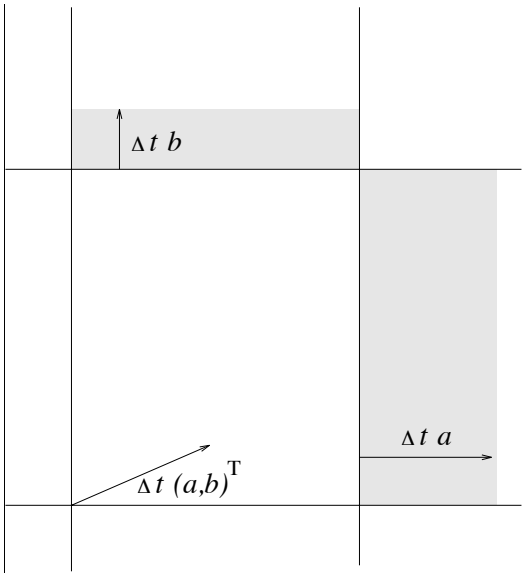

Figure 1: *Flux in dimensional splitting.*

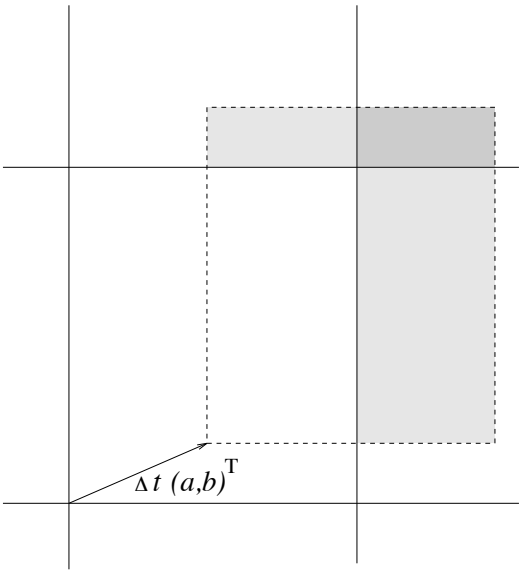

Figure 2: *Movement of all points with characteristic speed.*

as shown in the Figure 7. If we now restrict the domain of dependence to Ω_0 of one cell, then the function

$$h^u_{\Omega_0}(\mathbf{x},t,\Delta t) = \int_{\Omega_0} h(\mathbf{y},t)\,\delta(\mathbf{x}-(\mathbf{y}+\Delta t\mathbf{u}(\mathbf{y},t)))d\mathbf{y}. \tag{7}$$

represents the distribution or motion of the quantity h in Ω_0 after time Δt. The transport from this cell Ω_0 to any other domain, i.e. the neighbors Ω_i, can be computed as

$$f^u_{\Omega_0\Omega_i} := \int_{\Omega_i} h^u_{\Omega_0}(\mathbf{x},t,\Delta t)\,d\mathbf{x}.$$

The dashed line in Figure 2 shows the support of the function $h^u_{\Omega_0}$ for a constant velocity in the cell. The dark grey domain in the upper right corner indicates the contribution to the diagonal cell, a domain which has no finite boundary with the cell.

Note that during this transport process the conservation property of the equation is satisfied,

$$\begin{aligned}\int_{I\!R^N} h^u_{\Omega_0}(\mathbf{x},t,\Delta t)d\mathbf{x} &= \int_{I\!R^N}\int_{\Omega_0} h(\mathbf{y},t)\delta(\mathbf{x}-(\mathbf{y}+\Delta t\mathbf{u}(\mathbf{y})))d\mathbf{y}d\mathbf{x}\\ &= \int_{\Omega_0} h(\mathbf{y},t)\int_{I\!R^N}\delta(\mathbf{x}-(\mathbf{y}+\Delta t\mathbf{u}(\mathbf{y})))d\mathbf{x}d\mathbf{y}\\ &= \int_{\Omega_0} h(\mathbf{y},t)d\mathbf{y}.\end{aligned} \tag{8}$$

i.e. the integration of $h^u_{\Omega_0}$ gives the 'amount' of h within Ω_0.

In the report with A. Schroll [11] we prove convergence of this type of scheme for scalar conservation laws. The same idea, in the context of kinetic theory can be found in [14]. The transport collapse operator described by K. W. Morton and P. N. Childs in [3] and the rotated Riemann solver proposed by R. LeVeque [16] as well as the multidimensional method introduce by P. Collela [4] lead to the same first order approximation if applied to a scalar conservation law. The extension to a higher order method is straith forward and does not need an additional

time integration step nor is it restricted to second order as the dimensional splitting approach (see [8]).

In a finite volume discretisation, the update of the mean value in a cell at time $t + \Delta t$ can be done by adding all in- and outgoing fluxes:

$$h^{n+1}_{\Omega_0} = h^n_{\Omega_0} - \frac{1}{|\Omega_0|} \sum_{j=1}^{k} \left(f^u_{\Omega_0 \Omega_j} - f^u_{\Omega_j \Omega_0} \right) = \frac{1}{|\Omega_0|} \sum_{j=0}^{k} f^u_{\Omega_j \Omega_0}. \tag{9}$$

Here, Ω_0 denotes the domain of the central cell and Ω_j are its neighbors. $|\Omega_0|$ is the volume of domain Ω_0.

3 The 1-D Riemann problem and its solution

There exist a lot of numerical methods to solve the Euler equations in one space dimension. We will briefly describe some of these methods and show the difficulties adapting them to two or more space dimensions.

The Euler equations describe a compressible fluid flow without viscous effects. In one space dimension they have the form:

$$\frac{\partial}{\partial t}\mathbf{U}(x,t) + \frac{\partial}{\partial x}\mathbf{F}(\mathbf{U}(x,t)) = 0 \qquad x \in I\!R,\ t > 0. \tag{10}$$

Here, $\mathbf{U}$ is the vector of conserved quantities and $\mathbf{F}$ is the flux of $\mathbf{U}$. They are given by

$$\mathbf{U} = \begin{pmatrix} \rho \\ m \\ E \end{pmatrix}; \qquad \mathbf{F}(\mathbf{U}) = \begin{pmatrix} m \\ um + p \\ u(E+p) \end{pmatrix}$$

where ρ denotes the density, m is the momentum, $u = m/\rho$ the velocity of the fluid, E is the total energy and p is the pressure. To complete the system of equations we need to add the equation of state. For an ideal gas it reads

$$p = (\gamma - 1)\left(E - \frac{m^2}{2\rho} \right). \tag{11}$$

To take discontinuous solutions into account one introduce the class of weak solutions in the mathematical formulation [25]. Hence, numerical methods that can capture shocks are necessary. In particular, solutions with discontinuous initial conditions $\mathbf{U}_0(x)$ must be allowed. Problems with such initial conditions are called Riemann problems (RP) and play an important role in the construction of numerical methods. The exact or approximate solution to these RP, defined by (10) and initial conditions

$$\mathbf{U}(x,0) = \mathbf{U}_0(x) = \begin{cases} \mathbf{U}_L & \text{if} \quad x < 0 \\ \mathbf{U}_R & \text{if} \quad x > 0 \end{cases} \tag{12}$$

are at the center of most numerical methods.

The classical Godunov Method [12] introduces such a RP at each cell interface and use this solution to update the unknown function. Since the solutions to the RP's are self similar, i.e. constant along the rays $x/t = const$, the constant value $\mathbf{U}^*$ along $x/t = 0$ determines the flux at the origin. The complexity of the full solution of a RP is the main drawback of Godunovs method.

In [20], Roe introduces some simplifications, to obtain an approximation of $\mathbf{U}^*$. He uses the linearized form of (10)

$$\frac{\partial}{\partial t}\mathbf{U} + \frac{\partial \mathbf{F}}{\partial \mathbf{U}}\frac{\partial}{\partial x}\mathbf{U} = \frac{\partial}{\partial t}\mathbf{U} + \mathbf{A}\frac{\partial}{\partial x}\mathbf{U} = 0.$$

Instead of solving the full non-linear RP, he replaces the Jacobian matrix $\mathbf{A}$ by a matrix $\mathbf{A}(\mathbf{U}_R, \mathbf{U}_L)$ such that

$$\mathbf{A}(\mathbf{U}_R, \mathbf{U}_L)(\mathbf{U}_R - \mathbf{U}_L) = \mathbf{F}(\mathbf{U}_R) - \mathbf{F}(\mathbf{U}_L)$$

holds. It turns out, that this matrix $\mathbf{A}(\mathbf{U}_R, \mathbf{U}_L)$ is equal to the Jacobian $\mathbf{A}$ evaluated at a special value $\tilde{\mathbf{U}} = \tilde{\mathbf{U}}(\mathbf{U}_R, \mathbf{U}_L)$, called Roe average. Because of this, the matrix $\mathbf{A}(\mathbf{U}_R, \mathbf{U}_L)$ has real eigenvalues and a full set of eigenvectors. Thus, $\mathbf{A}(\mathbf{U}_R, \mathbf{U}_L)$ can be diagonalized and the flux-difference

$$\begin{aligned} \mathbf{F}(\mathbf{U}_R) - \mathbf{F}(\mathbf{U}_L) &= \mathbf{A}(\mathbf{U}_R, \mathbf{U}_L)(\mathbf{U}_R - \mathbf{U}_L) \\ &= \mathbf{S}\Gamma\mathbf{S}^{-1}(\mathbf{U}_R - \mathbf{U}_L) \\ &= \sum_{i=1}^{3} \mathbf{s}_i \gamma_i \beta_i \end{aligned}$$

can be replaced by a linear combination of the eigenvectors $\mathbf{s}_i$ of $\mathbf{A}(\mathbf{U}_R, \mathbf{U}_L)$ moving with the speed γ_i, the corresponding eigenvalue. The non-linear waves like shocks, contact discontinuities (CD) and rarefaction wave are replaced by a linear combination of the eigenvectors of $\mathbf{A}(\mathbf{U}_R, \mathbf{U}_L)$. The choice of the value $\tilde{\mathbf{U}}$ allows the method to capture steady shocks and contact surfaces, as the Godunov Method does.

The main disadvantage of both approaches, is the dependence of the intermediate values $\mathbf{U}^*$ and $\tilde{\mathbf{U}}$ on both states $\mathbf{U}_R$ and $\mathbf{U}_L$. In one space dimension, each cell interface is uniquely related to two states. This is not true in several space dimensions, unless a dimensional splitting is used. But this is to be avoided, because of the strong dependence on the underlying grid, as mentioned before. Without the use of the normal directions the fluxes depend on more than two states, and it is not obvious how to chose $\mathbf{U}_R$ and $\mathbf{U}_L$ in this case.

Another class of schemes uses the homogeneity of the Euler equations . For the flux $\mathbf{F}$ we have the special relation

$$\mathbf{F}(\mathbf{U}) = \frac{\partial \mathbf{F}}{\partial \mathbf{U}}\mathbf{U} := \mathbf{A}\mathbf{U}. \tag{13}$$

The flux is decomposed into the eigenvectors of the Jacobian matrix $\mathbf{A}$. This procedure is called flux vector splitting. It is important to understand this idea in more detail for the derivation of the new method. Since the Euler equations are hyperbolic the eigenvalues of the Jacobian matrix of $\mathbf{F}$ are all real with a complete set of eigenvectors. Let

$$\mathbf{R} = (\mathbf{r}_1, \mathbf{r}_2, \mathbf{r}_3)$$

be the matrix of right eigenvectors, $\mathbf{r_i}$, of $\mathbf{A}$. Then, the flux $\mathbf{F}$ can be rewritten in the form

$$\mathbf{F}(\mathbf{U}) = \mathbf{A}\mathbf{U} = \mathbf{R}\mathbf{\Lambda}\mathbf{R}^{-1}\mathbf{U} = \sum_{i=1}^{3} \mathbf{r}_i \lambda_i \alpha_i. \tag{14}$$

Here, $\mathbf{\Lambda} = \mathrm{diag}(\lambda_1, \lambda_2, \lambda_3)$ is a diagonal matrix and $(\alpha_1, \alpha_2, \alpha_3)^T = \mathbf{R}^{-1}\mathbf{U}$ a given vector. Since $\mathbf{U} = \mathbf{R}\,\mathbf{R}^{-1}\,\mathbf{U}$ can be decomposed into the same vectors $\mathbf{r}_i\alpha_i$, the flux $\mathbf{F}$ can be identified by a motion of these three waves traveling with speed λ_i. This decomposition is called Steger-Warming splitting [26]. A symbolic representation is sketched in Figure 3.

For an ideal gas, i.e. a gas with constant heat capacities and the equation of state (11), the matrix $\mathbf{A}$ has the form

$$\mathbf{A} = \begin{pmatrix} 0 & 1 & 0 \\ (\gamma-3)\frac{u^2}{2} & (3-\gamma)u & (\gamma-1) \\ \left((\gamma-1)\frac{u^2}{2} - H\right)u & H-(\gamma-1)u^2 & \gamma u \end{pmatrix}$$

with eigenvalues $\mathbf{\Lambda} = \mathrm{diag}(u-c, u, u+c)$. The speed of sound c is given by $c^2 = \gamma p/\rho$; $H = (E+p)/\rho$ is the total enthalpy and $\gamma = c_p/c_v$ is the ratio of the heat capacities for constant pressure and constant volume. The eigenvectors are

$$\mathbf{R} = \begin{pmatrix} 1 & 1 & 1 \\ u-c & u & u+c \\ H-uc & \frac{u^2}{2} & H+uc \end{pmatrix} \tag{15}$$

and the vector $\mathbf{R}^{-1}\mathbf{U}$ has the simple form

$$\begin{pmatrix} \alpha_1 \\ \alpha_2 \\ \alpha_3 \end{pmatrix} = \mathbf{R}^{-1}\mathbf{U} = \frac{\rho}{2\gamma}\begin{pmatrix} 1 \\ 2(\gamma-1) \\ 1 \end{pmatrix}. \tag{16}$$

Assuming, that different waves do not interact (super position), the flux over one cell boundary can be described in the following way: First, decompose the state vector $\mathbf{U}_R$ and $\mathbf{U}_L$ as a linear combination of the eigenvectors. With (14), the flux $\mathbf{F}(\mathbf{U}_L)$ and $\mathbf{F}(\mathbf{U}_R)$ is given as these eigenvectors times the corresponding eigenvalues. Second, use only this part of $\mathbf{F}(\mathbf{U}_L)$ that crosses the cell boundary to the right, i.e. waves with positive speed. Similarly, the waves with negative speed of $\mathbf{F}(\mathbf{U}_R)$ are taken into account. Hence, the complete flux over the cell interface between $\mathbf{U}_L$ and $\mathbf{U}_R$ is given by

$$\begin{aligned} \mathbf{F}(\mathbf{U}_L, \mathbf{U}_R) &= \sum \mathbf{r}_i^L \max(0, \lambda_i^L)\alpha_i^L + \sum \mathbf{r}_i^R \min(0, \lambda_i^R)\alpha_i^R \\ &=: \mathbf{F}^+(\mathbf{U}_L) + \mathbf{F}^-(\mathbf{U}_R). \end{aligned}$$

This is an easy way to calculate the flux across cell boundaries and is based more or less on the same idea of transport as described previously in the scalar case. We have thus shown that in the one-dimensional case it is possible, to decompose the flux into a finite number of advection processes.

The advantage here is, that the total flux is a linear combination of fluxes depending on only one state, either $\mathbf{U}_R$ or $\mathbf{U}_L$. This can simply be generalized to several space dimensions by taking into account the additional fluxes due to additional neighboring cells. Unfortunately, a simple decomposition of the flux $\mathbf{F}(\mathbf{U})$ in (14) and the state vector $\mathbf{U}$ is not possible in two or more space dimensions. The two Jacobian matrices in x- and y-direction can not be diagonalized simultaneously. Hence, there is no linearization as in one space dimension.

4 The Method of Transport

In this section we will derive the multi-dimensional method for the Euler equations. The idea is to use the transport process as described in the scalar case combined with a modification of the flux vector splitting from the previous section. To meet this goal, we have to solve the following problems:

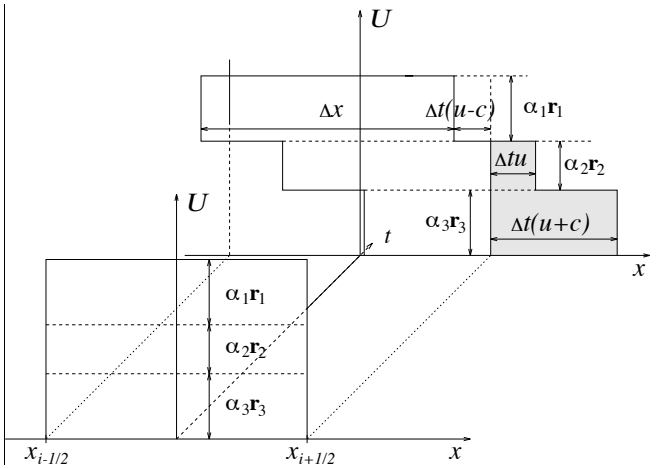

Figure 3: *Decomposition of the state vector* **U** *in the eigenvectors and the resulting flux in each component.*

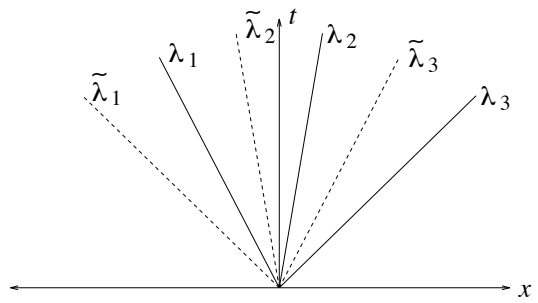

Figure 4: *The reflection of the space exchanges the waves corresponding to the eigenvalues* λ_1 *and* λ_3.

b) Find quantities, like the eigenvectors of **A** in 1-D, that decompose the state vector **U** and the multi-dimensional flux in a linear way as in (14).

In the next sections we will use the following notation: bold face characters denote vectors or matrices, italic letters denote scalars. We define the velocity vector $\mathbf{u} = (u, v)^T$ and the momentum $\mathbf{m} = (m, n)^T$.

4.1 Properties of the Euler equations

To solve the above problems, we will use the following well known properties of the Euler equations

a) (Invariance under reflection)
The one-dimensional Euler equations are invariant with respect to a reflection in space, i.e. a transformation $\tilde{x} = -x$. If $\mathbf{U}(x,t)$ is a solution to (10) then the function

$$\tilde{\mathbf{U}}(\tilde{x},t) = \begin{pmatrix} \rho(\tilde{x},t) \\ \rho\tilde{u}(\tilde{x},t) \\ E(\tilde{x},t) \end{pmatrix} = \begin{pmatrix} \rho(-x,t) \\ -\rho u(-x,t) \\ E(-x,t) \end{pmatrix}$$

is a solution of (10), too.

b) (Invariance under rotation)
The two-dimensional Euler equations are invariant with respect to a rotation of the coordinate system. Let $\mathbf{U}(\mathbf{x},t)$ be a solution to (17), $\mathbf{x} \in I\!R^2$, $t \in I\!R^+$. Then, for each $\alpha \in I\!R$, $\tilde{\mathbf{U}}(\tilde{\mathbf{x}},t) = \tilde{\mathbf{D}}(\alpha)\mathbf{U}(\mathbf{D}(\alpha)\mathbf{x},t)$ with

$$\mathbf{D}(\alpha) = \begin{pmatrix} \cos(\alpha) & -\sin(\alpha) \\ \sin(\alpha) & \cos(\alpha) \end{pmatrix}; \qquad \tilde{\mathbf{D}}(\alpha) = \begin{pmatrix} 1 & 0 & 0 & 0 \\ 0 & & & 0 \\ 0 & & \mathbf{D}(\alpha) & 0 \\ 0 & 0 & 0 & 1 \end{pmatrix}$$

is a solution of (17), too.

The two dimensional Euler equations have the form

$$\frac{\partial \mathbf{U}}{\partial t} + \frac{\partial \mathbf{F}}{\partial x} + \frac{\partial \mathbf{G}}{\partial y} = 0, \tag{17}$$

with

$$\mathbf{U} = \begin{pmatrix} \rho \\ m \\ n \\ E \end{pmatrix}, \quad \mathbf{F}(\mathbf{U}) = \begin{pmatrix} m \\ um + p \\ un \\ u(E+p) \end{pmatrix}, \quad \mathbf{G}(\mathbf{U}) = \begin{pmatrix} n \\ vm \\ vn + p \\ v(E+p) \end{pmatrix}. \tag{18}$$

n is the momentum and $v = n/\rho$ the velocity in the y-direction.

The second property answers the question about the characteristic directions. It shows that unlike the scalar case with only one defined propagation direction, we get the well know Monge cone as a characteristic surface and the fluid velocity as the center of the sphere.

From the first property, we derive the following result. Since the equations are invariant under a reflection, the characteristic related to λ_3 of the solution $\mathbf{U}$ at some point transforms into $-\lambda_3 = -u - c = \tilde{u} - c = \tilde{\lambda}_1$, i.e. into the characteristic $\tilde{\lambda}_1$ of solution $\tilde{\mathbf{U}}$. The two characteristics switch with the transformation, which indicates, that both of them have something in common. This becomes obvious in the 2-D case. Now, the two curves are connected via the Monge cone.

We are looking for a new interpretation of the vectors $\alpha_1 \mathbf{r}_1$ and $\alpha_3 \mathbf{r}_3$, that is independent of the space dimension. The two vectors are almost the same. We can write them in the form

$$(\alpha \mathbf{r})_{1,3} = \mathbf{a} \pm \mathbf{b}$$

with

$$\mathbf{a} = \frac{\rho}{2\,\gamma} \begin{pmatrix} 1 \\ u \\ H \end{pmatrix} = \frac{1}{2}(\alpha_1 \mathbf{r}_1 + \alpha_3 \mathbf{r}_3) \quad \text{and} \quad \mathbf{b} = \frac{\rho\, c}{2\,\gamma} \begin{pmatrix} 0 \\ 1 \\ u \end{pmatrix} = \frac{1}{2}(\alpha_1 \mathbf{r}_1 - \alpha_3 \mathbf{r}_3) \tag{19}$$

With this notation, part $\mathbf{a}$ moves along both characteristic directions. With $n_{1,3} = \pm 1$ and $\lambda_{1,3} = u \pm c$, we obtain for the propagation in the flux vector setting,

$$\mathbf{a}\,(u + n_i\, c) \quad \text{and} \quad n_i\, \mathbf{b}\,(u + n_i\, c).$$

The sum of both parts for $i = 1, 3$ recovers the original splitting (14), since

$$\sum_{i \in \{1,3\}} (\mathbf{a} + n_i\, \mathbf{b})(u + n_i\, c) = \sum_{i \in \{1,3\}} \alpha_i\, \mathbf{r}_i\, \lambda_i.$$

In the generalization to two space dimensions, we replace $n_{1,3}$ by the vector $\mathbf{n}$ on the surface of the unit sphere S and the sum over both directions by an integral over this sphere. Then the points with

$$\mathbf{u} + \mathbf{n}\, c \qquad \forall \mathbf{n} \in S$$

represent the characteristic hyper-surface mentioned in property b).

4.2 Mathematical Description

In the previous sections we recalled different numerical schemes together with physical properties of the equations we want to solve. We wanted to motivate the definitions and formulas following in this section. It turns out that the basic ideas of this approach provide more insight into the behavior of multi-dimensional flow than just the resulting numerical method in section 4.3.2. Thus it seem as important to us to explain the ideas as to state the results.

We now define functions, which we call waves, that reflect the physical behavior of the equations, i.e. allow infinitely many propagation directions embedded in a conservative finite volume approach.

First, we define the wave related to the single propagation direction $\mathbf{u}$.

Definition 1 *(Wave $\mathcal{U}$)*

With the vector function

$$\mathbf{R}_2(\mathbf{U}) := \frac{\gamma - 1}{\gamma} \begin{pmatrix} \rho \\ \rho\mathbf{u} \\ \rho|\mathbf{u}|^2/2 \end{pmatrix} \tag{20}$$

the wave $\mathcal{U}$ is defined as the transformation of $\mathbf{R}_2$ on domain Ω_0 at time t, after a time step Δt. More precisely,

$$\mathcal{U}_{\Omega_0}(\mathbf{x}, t, \Delta t) = \int\limits_{\Omega_0} \mathbf{R}_2(\mathbf{U}(\mathbf{y}, t))\delta(\mathbf{x} - (\mathbf{y} + \Delta t\mathbf{u}(\mathbf{y}, t)))d\mathbf{y}. \tag{21}$$

Figure 5 shows the wave $\mathcal{U}$ for constant values in the cell Ω_0. The dark lines indicate the underlying grid. The contribution from domain Ω_0 to Ω_i within the time step Δt is given by

$$\begin{aligned} \mathbf{F}^u_{\Omega_0\Omega_i} &= \int\limits_{\Omega_i} \mathcal{U}_{\Omega_0}(\mathbf{x}, t, \Delta t)d\mathbf{x} \\ &= \int\limits_{\Omega_i}\int\limits_{\Omega_0} \mathbf{R}_2(\mathbf{U}(\mathbf{y}, t))\delta(\mathbf{x} - (\mathbf{y} + \Delta t\mathbf{u}(\mathbf{y}, t)))d\mathbf{y}d\mathbf{x}. \end{aligned} \tag{22}$$

Note, that for each component of $\mathbf{R}_2$ the component in (21) has exactly the structure of $h^u_{\Omega_0}$ in (7) for the scalar case, i.e. we are using the physical directions. The computation of the contributions $\mathbf{F}^u_{\Omega_0\Omega_i}$ involve only values at time level t.

The next definition is related to the part $\mathbf{a}$ in (19), that propagates in all directions. We set

Definition 2 *(Wave $\mathcal{C}$)*

With the vector function

$$\mathbf{R}_1(\mathbf{U}) := \frac{1}{\gamma} \begin{pmatrix} \rho \\ \rho\mathbf{u} \\ \rho H \end{pmatrix} \tag{23}$$

the wave $\mathcal{C}$ is defined as the transformation of $\mathbf{R}_1$ on domain Ω_0 at time t, after a time step Δt. More precisely,

$$\mathcal{C}_{\Omega_0}(\mathbf{x}, t, \Delta t) = \frac{1}{|O|}\int\limits_{O}\int\limits_{\Omega_0} \mathbf{R}_1(\mathbf{U}(\mathbf{y}, t))\delta(\mathbf{x} - (\mathbf{y} + \Delta t\,(\mathbf{u}(\mathbf{y}, t) + \mathbf{n}\,c(\mathbf{y}, t))))d\mathbf{y}dO.$$

Here, O is the set of all points on the unit sphere in $I\!R^N$; $|O|$ is the value of the surface area of the sphere, dO is a surface element and $\mathbf{n}$ is the outer unit normal to element dO. For a simpler notation we define the function $\mathbf{g}$ as

$$\mathbf{g}(\mathbf{y}, \mathbf{n}, t, \Delta t) := \mathbf{y} + \Delta t\,(\mathbf{u}(\mathbf{y}, t) + \mathbf{n}\,c(\mathbf{y}, t)).$$

Analogous to (22), we obtain the contribution from domain Ω_0 to Ω_i as

$$\begin{aligned}\mathbf{F}^{c}_{\Omega_0\Omega_i} &= \int\limits_{\Omega_i} \mathcal{C}_{\Omega_0}(\mathbf{x},t,\Delta t)d\mathbf{x} \\ &= \int\limits_{\Omega_i} \frac{1}{|O|}\int\limits_{O}\int\limits_{\Omega_0} \mathbf{R}_1(\mathbf{U}(\mathbf{y},t))\delta(\mathbf{x}-\mathbf{g}(\mathbf{y},\mathbf{n},t,\Delta t))d\mathbf{y}dOd\mathbf{x}.\end{aligned} \tag{24}$$

The same conservation property as in (8) is fulfilled by construction. Let h be one of the components of the vector $\mathbf{R}_1$ at time t, then each of the components of wave $\mathcal{C}$ has the structure

$$h^{c}_{\Omega_0}(\mathbf{x},t,\Delta t) = \frac{1}{|O|}\int\limits_{O}\int\limits_{\Omega_0} h(\mathbf{y},t)\delta(\mathbf{x}-\mathbf{g}(\mathbf{y},\mathbf{n},t,\Delta t))d\mathbf{y}dO.$$

and therefore

$$\begin{aligned}\int\limits_{I\!R^N} h^{c}_{\Omega_0}(\mathbf{x},t,\Delta t)d\mathbf{x} &= \int\limits_{I\!R^N} \frac{1}{|O|}\int\limits_{O}\int\limits_{\Omega_0} h(\mathbf{y},t)\delta(\mathbf{x}-\mathbf{g}(\mathbf{y},\mathbf{n},t,\Delta t))d\mathbf{y}dOd\mathbf{x} \\ &= \int\limits_{\Omega_0} h(\mathbf{y},t)\frac{1}{|O|}\int\limits_{O}\int\limits_{I\!R^N} \delta(\mathbf{x}-\mathbf{g}(\mathbf{y},\mathbf{n},t,\Delta t))d\mathbf{x}dOd\mathbf{y} \\ &= \int\limits_{\Omega_0} h(\mathbf{y},t)\frac{1}{|O|}\int\limits_{O} dOd\mathbf{y} \\ &= \int\limits_{\Omega_0} h(\mathbf{y},t)d\mathbf{y}.\end{aligned}$$

Figure 6 indicates the quantitative behavior of wave $\mathcal{C}$ after time $\Delta t\, c = 0.4\Delta x$. The normalized amplitude of the components is shown, assuming constant functions in the domain Ω_0. The dark lines indicate the underlying grid and separate the contributions to different cells.

The last wave is related to the part **b** in (19). To be consistent with the Euler equations, we have to introduce a new structure.

Definition 3 *(Wave $\mathcal{C}^-$)*

Let $\mathbf{I}$ *be the unit matrix and* $\mathbf{0}$ *the vector of zeros in the space* $I\!R^N$*. Using the* $(N+2)\times N$ *matrix*

$$\mathbf{L}(\mathbf{U}) := \frac{\rho c}{\gamma}\begin{pmatrix}\mathbf{0}^T\\ \mathbf{I}\\ \mathbf{u}^T\end{pmatrix}, \tag{25}$$

the wave $\mathcal{C}^-$ *is defined as*

$$\mathcal{C}^{-}_{\Omega_0}(\mathbf{x},t,\Delta t) = \frac{N}{|O|}\int\limits_{O}\int\limits_{\Omega_0} \mathbf{L}(\mathbf{U}(\mathbf{y},t))\cdot\mathbf{n}\,\delta(\mathbf{x}-\mathbf{g}(\mathbf{y},\mathbf{n},t,\Delta t))d\mathbf{y}dO.$$

The expressions for the contribution from one domain to another domain are the same.

$$\begin{aligned}\mathbf{F}^{c-}_{\Omega_0\Omega_i} &= \int\limits_{\Omega_i} \mathcal{C}^{-}_{\Omega_0}(\mathbf{x},t,\Delta t)d\mathbf{x} \\ &= \int\limits_{\Omega_i} \frac{N}{|O|}\int\limits_{O}\int\limits_{\Omega_0} \mathbf{L}(\mathbf{U}(\mathbf{y},t))\cdot\mathbf{n}\,\delta(\mathbf{x}-\mathbf{g}(\mathbf{y},\mathbf{n},t,\Delta t))d\mathbf{y}dOd\mathbf{x}.\end{aligned} \tag{26}$$

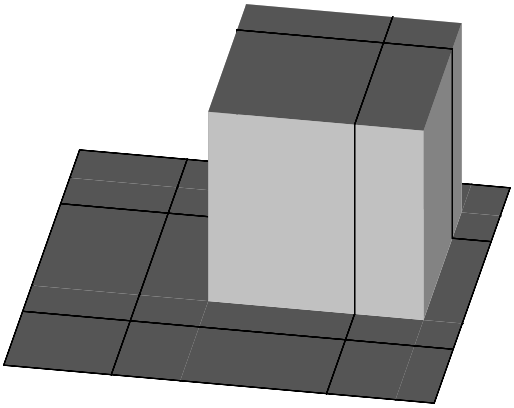

Figure 5: *Wave $\mathcal{U}$ generated from the center cell at time $\Delta t = 1$ with velocity $\mathbf{u} = (0.3, 0.2)^T$ and constant states at time t.*

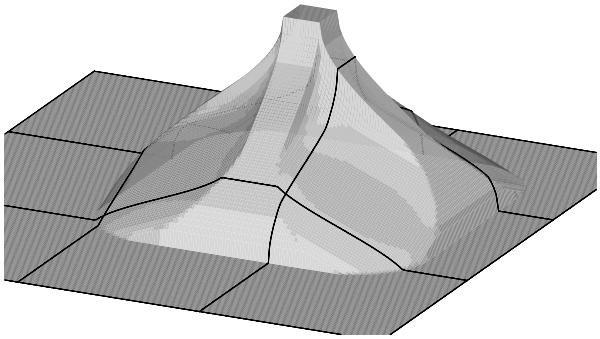

Figure 6: *Wave $\mathcal{C}$ generated from the center cell at time $\Delta t = 1$ with velocity $\mathbf{u} = (0.3, 0.2)^T$ and $c = 0.4$ and constant states at time t.*

With these relations, the total contribution from domain Ω_0 to Ω_i is given as the sum of the parts related to the different waves,

$$\mathbf{F}_{\Omega_0\Omega_i} = \mathbf{F}^u_{\Omega_0\Omega_i} + \mathbf{F}^c_{\Omega_0\Omega_i} + \mathbf{F}^{c-}_{\Omega_0\Omega_i}. \tag{27}$$

This leads to the form in (9). Using the same notation it reads:

$$\mathbf{U}^{n+1}_{\Omega_0} = \mathbf{U}^n_{\Omega_0} - \frac{1}{|\Omega_0|}\sum_{i=1}^{k}(\mathbf{F}_{\Omega_0\Omega_i} - \mathbf{F}_{\Omega_i\Omega_0}) = \frac{1}{|\Omega_0|}\sum_{i=0^k}\mathbf{F}_{\Omega_i\Omega_0}. \tag{28}$$

For the above defined numerical scheme we state the following result:

Theorem 1 *(Consistency of Contributions)*

The numerical scheme in (28)*, with the waves $\mathcal{U}$, $\mathcal{C}$ and $\mathcal{C}^-$ in Definition 1–3 and their contributions in* (22)*,* (24) *and* (26)*, is consistent with the Euler equations in the sense, that the physical flux $\mathbf{F}$ and $\mathbf{G}$ in* (18) *can be written as*

$$\begin{aligned}\Delta t\Delta y\mathbf{F}(\mathbf{U}) &= \mathbf{F}_{\Omega_0\Omega_2} + \mathbf{F}_{\Omega_0\Omega_3} + \mathbf{F}_{\Omega_0\Omega_4} - \mathbf{F}_{\Omega_2\Omega_0} - \mathbf{F}_{\Omega_3\Omega_0} - \mathbf{F}_{\Omega_4\Omega_0}\\ \Delta t\Delta x\mathbf{G}(\mathbf{U}) &= \mathbf{F}_{\Omega_0\Omega_8} + \mathbf{F}_{\Omega_0\Omega_1} + \mathbf{F}_{\Omega_0\Omega_2} - \mathbf{F}_{\Omega_8\Omega_0} - \mathbf{F}_{\Omega_1\Omega_0} - \mathbf{F}_{\Omega_2\Omega_0}\end{aligned}$$

for all uniform functions $\mathbf{U}$*.*

A more general definition of multi-dimensional waves and transport methods in the above sense can be found in [10]. The proof of a more general theorem is shown in [6]. In the one-dimensional case, the method reduces to the Steger Warming flux vector splitting.

4.3 Numerical Implementation

In order to construct the 2-D method from equations (22)–(26), we restrict ourselves to a cartesian grid as in the scalar case. We start with wave $\mathcal{U}$ using the same notation as before. Thus Ω_0 denotes the central cell i, j and the domains Ω_1,...,Ω_8 surround it clockwise. Since all the quantities are constant within the cell, the integration in Definition 1 contains only the δ-function. $\mathcal{U}_{\Omega_0}$ is given by

$$\mathcal{U}_{\Omega_0}(\mathbf{x}, t, \Delta t) = \mathbf{R}_2(\mathbf{U})\int_{\Omega_0}\delta(\mathbf{x} - (\mathbf{y} + \Delta t\mathbf{u}))d\mathbf{y} = \mathbf{R}_2(\mathbf{U})l_{\Omega_0}(\mathbf{x} - \Delta t\mathbf{u}),$$

where $l_{\Omega_0}(\mathbf{x})$ is defined as

$$l_{\Omega_0}(\mathbf{x}) = \begin{cases} 1 & \text{if} \quad \mathbf{x} \in \Omega_0 \\ 0 & \text{otherwise} \end{cases} .$$

The contribution from domain Ω_0 to Ω_i can be computed, i.e. for the diagonal part we get

$$F^u_{\Omega_0\Omega_2} = (\Delta t)^2 \mathbf{R}_2(\mathbf{U}) \max(0, u) \max(0, v).$$

Note, that

- this part does not appear in a splitting method. It is approximated by two fluxes, first in x- then in y-direction.
- it is divided by the volume of the cell in the final formula. Thus, the contribution is multiplied by $\Delta t/\Delta x$ and $\Delta t/\Delta y$ which is usually kept constant in a convergence analysis.

This means, the contribution in the diagonal cell, i.e. to a domain without cell interface, is of the same order as the one across the cell interface. It is not a second order influence and thus important near discontinuities disalligned with the cell surfaces.

For wave $\mathcal{C}$, the assumption of constant states in (24) allows the integration of the δ-function. In two space dimensions $|O| = 2\pi$. The normal unit vector has the simple form $\mathbf{n} = (\cos(\alpha), \sin(\alpha))^T$, where α is the angle to the positive x-direction. With Definition 2 and the step-function l_{Ω_0} we can write wave $\mathcal{C}$ as

$$\mathcal{C}_{\Omega_0}(\mathbf{x}, t + \Delta t) = \frac{1}{2\pi} \mathbf{R}_1(\mathbf{U}) \int_{-\pi}^{\pi} l_{\Omega_0}(\mathbf{x} - \Delta t(\mathbf{u} + c\mathbf{n}(\alpha))) d\alpha.$$

Using the linear substitution $\mathbf{z} = \mathbf{x} - \Delta t \mathbf{u}$, the movement with velocity $\mathbf{u}$ can be eliminated. Thus the integration and the shape of wave $\mathcal{C}$ is independent of $\mathbf{u}$. We get

$$\mathcal{C}_{\Omega_0}(\mathbf{z} + \Delta t\mathbf{u}, t + \Delta t) = \frac{1}{2\pi} \mathbf{R}_1(\mathbf{U}) \underbrace{\int_{-\pi}^{\pi} l_{\Omega_0}(\mathbf{z} - \Delta t c\, \mathbf{n}(\alpha)) d\alpha}_{I_{\Omega_0}(\mathbf{z}, \Delta t)} . \tag{29}$$

The support of wave $\mathcal{C}$ (see Fig. 6) decouples into a number of subdomains, each with a different representation of $\mathcal{C}$. In Fig. 7 the solid lines show the subdomains, the dashed lines indicate the underlying grid and the dotted lines denote the motion of the domain Ω_0 with velocity $\mathbf{u}$. With a nonzero fluid velocity we get

$$\mathcal{C}_{\Omega_0}(\mathbf{x}, \Delta t) = \mathbf{R}_1(\mathbf{U}) \frac{1}{2\pi} I_{\Omega_0}(\mathbf{x} - \Delta t\mathbf{u}, \Delta t).$$

Using this function $I_{\Omega_0}(\mathbf{x}, \Delta t)$, the contribution from domain Ω_0 to any other domain Ω_i can be calculated as

$$F^c_{\Omega_0\Omega_2} = \mathbf{R}_1(\mathbf{U}) \frac{1}{2\pi} \int_{\Omega_2} I_{\Omega_0}(\mathbf{x} - \Delta t\mathbf{u}, \Delta t) d\mathbf{x}. \tag{30}$$

The function I is separable with respect to both space variables, so that we can write I in the form:

$$I(x, y, \Delta t) = g_1(x) + g_2(y) + g_0$$

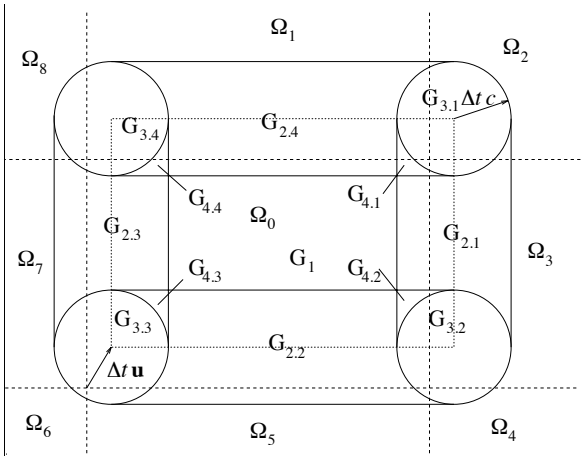

Figure 7: *Decomposition of the support of wave $\mathcal{C}$ in domains with the same function.*

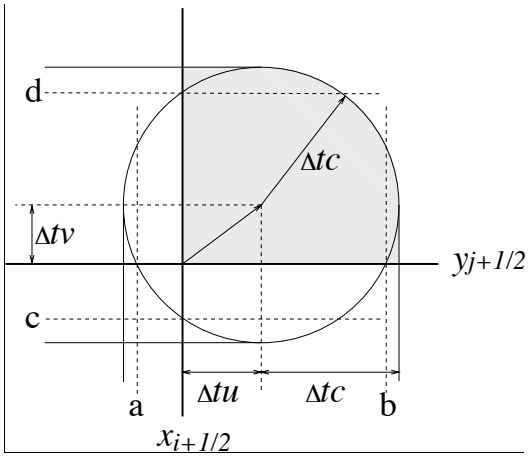

Figure 8: *Calculation of the flux for wave $\mathcal{C}$.*

Figure 8 shows one possible integration pattern. The structure of the function I allows the analytic integration in all subdomains. The same holds for wave $\mathcal{C}^-$. Hence, we obtain explicit expressions for the contributions $\mathbf{F}^{c}_{\Omega_0\Omega_i}$ and $\mathbf{F}^{c^-}_{\Omega_0\Omega_i}$. The interested reader is referred to [6] for a detailed description of these functions.

To calculate the value within a cell at the next timestep, we use (27) and (28) from the previous sections.

5 Numerical Experiments

The numerical method derived in the previous section has been tested on a large number of problems. To compare with existing methods, solutions where computed, using the Van Leer method and other methods with dimensional splitting. Since all the methods are of first order, there are only small differences in most of the examples with weak shocks or rarefaction waves. The second problem discussed here is an exception to this rule. The last calculation deals with a Mach 10 flow to test the robustness of the method. We denote with (MoT) the derived method of transport, and with (VL) the Van Leer flux vector splitting method.

The first example is a two-dimensional Riemann problem. As initial conditions we choose constant states in each quadrant. Neighboring quadrants are connected by a simple wave, in this case by two slip lines and two rarefaction waves. The initial conditions are

$$\begin{array}{llll} \rho = 0.5197 & p = 0.4 & u = -0.6259 & v = 0.1 \quad \text{if} \quad x < 0, y > 0 \\ \rho = 0.8 & p = 0.4 & u = 0.1 & v = 0.1 \quad \text{if} \quad x > 0, y > 0 \\ \rho = 1.0 & p = 1.0 & u = 0.1 & v = 0.1 \quad \text{if} \quad x < 0, y < 0 \\ \rho = 0.5197 & p = 0.4 & u = 0.1 & v = -0.6258 \quad \text{if} \quad x > 0, y < 0 \end{array}$$

The cartesian grid used has 400×400 points. The shock thickness in Figure 9 and 10 for the MoT and VL is nearly the same.

The next example includes two weak shocks and two slip lines. The initial conditions are

$$\begin{array}{llll} \rho = 0.5313 & p = 0.4 & u = 0.0 & v = 0.0 \quad \text{if} \quad x < 0, y > 0 \\ \rho = 1.0 & p = 1.0 & u = 0.7276 & v = 0.0 \quad \text{if} \quad x > 0, y > 0 \\ \rho = 0.8 & p = 1.0 & u = 0.0 & v = 0.0 \quad \text{if} \quad x < 0, y < 0 \\ \rho = 1.0 & p = 1.0 & u = 0.0 & v = 0.7276 \quad \text{if} \quad x > 0, y < 0 \end{array}$$

A second look at the results (Fig. 11, 12) shows large differences in the structure of the shock. The solution of the multidimensional method (Fig. 13) shows two Mach reflections and two contact surfaces at the intersection of the four shocks. VL shows one curved shock connected with two others. This explains the large density behind the shock in VL.

There is no exact solution to this problem. However, a qualitative result can be obtained using shock polars. Since the solution is symmetric with respect to the line $x = y$ and self similar, the transformation

$$x' = \frac{1}{\sqrt{2}}(x+y) + s\,t, \quad y' = \frac{1}{\sqrt{2}}(y-x)$$

puts the shock shock interaction point at rest, if s is the speed of the shock between quadrant 1 and 3. Since the shock speed is determined from the one dimensional problems, it is constant in time. Hence, we can use the model of shock reflections as a first approximation. It turns out, that for an angle of 45^o, there is no regular reflection. The highest possible angle for these conditions is 40.8^o, with a density of 1.835 behind the reflected shock, i.e. a situation as in Figure 12. Using the 45^o angle of incidence, we obtain a Mach reflection with a density of 1.66 behind the reflected shock and 1.52 behind the Mach stem [1]. This seem to indicates, that the solution obtained with VL is wrong, and MoT shows the proper behavior.

Example 1: Iso density contours, $\Delta\rho = 0.02$.

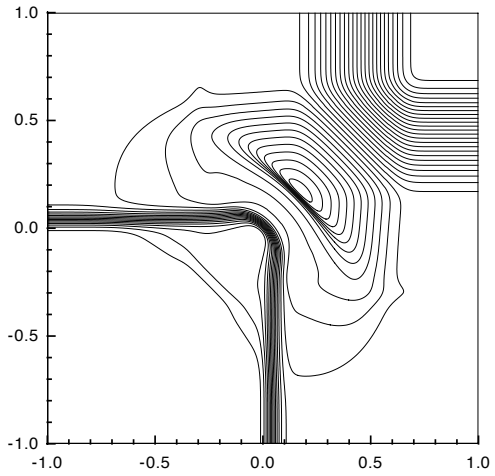

Figure 9: *MoT, Min.:* 0.2795

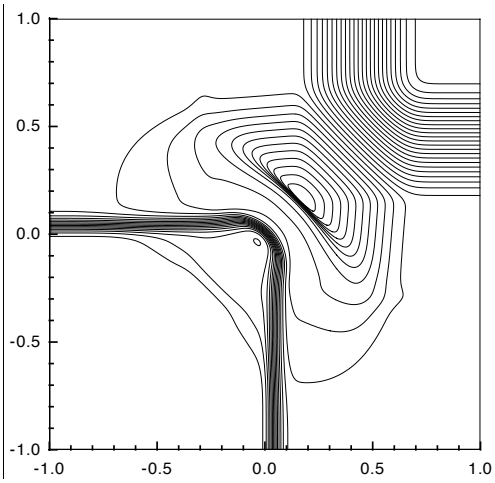

Figure 10: *VL, Min.:* 0.271

Example 2: Iso density contours: $\Delta\rho = 0.04$.

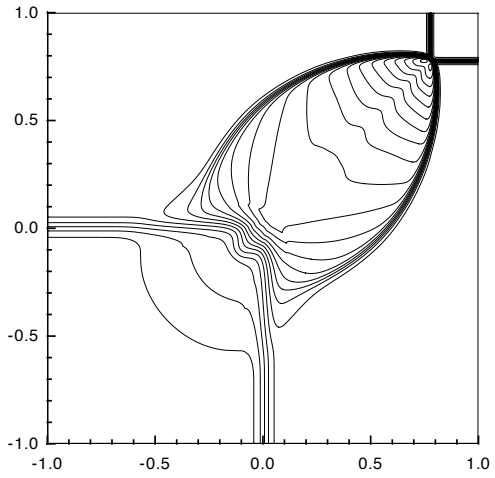

Figure 11: *MoT, Max.:* 1.721

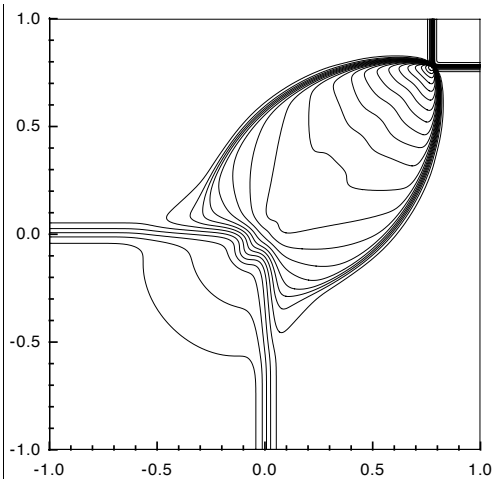

Figure 12: *VL, Max.:* 1.820

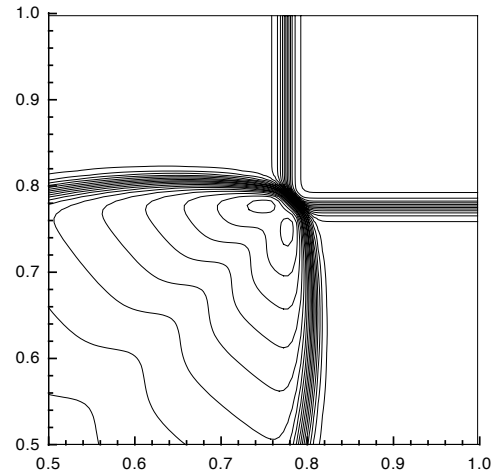

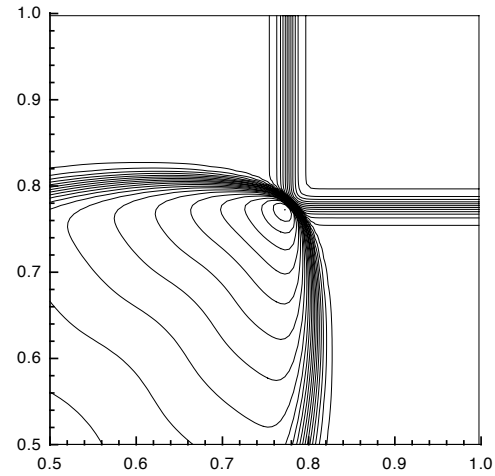

Figure 13: *Enlargement for MoT and VL.*

The last two examples show a steady shock reflections. First we show the solution for the weak Mach 1.4 shock in [4]. The domain is $[-2,2]\times[0,1]$ and we use 60×20 points. The CFL-Number for both methods (MoT and VL) is 0.9. Figure 14 shows the density at $y = 0.525$. The shocks are sharper for MoT. This is a multi-dimensional effect. The profile for the 1-D steady normal shock is sharper for VL (see Figure 15). Hence, the dimensional splitting approach introduces more numerical viscosity than the unsplit method.

The last problem includes a strong Mach 10 shock. The values of the analytic solution are:

quantity	left	middle	right
ρ	1.0	5.714285714285714	18.18385326582769
p	1.0	116.5	748.0377039786476
u	23.66431913239847	18.78355331134129	16.70442203362488
v	0.0	-8.453734381916670	1.8e-14

The domain in this problem is $[-1.73, 4.07]\times[0,1]$ with a grid of 120×20 points. We observed the following difference between MoT and VL. First, to obtain a solution with VL, we had to reduce the time step to $CFL \leq 0.7$. Second, VL fails to recover the value of density and momentum after the reflection (see Figure 16) next to the wall. This leads to a small shift of the second shock front (see Figure 17). The shock thickness is smaller for MoT, as in the weak shock case. For comparison, both calculations were done with the reduced time step. This is not necessary for MoT. The solution is exactly the same, even with $CFL = 0.95$.

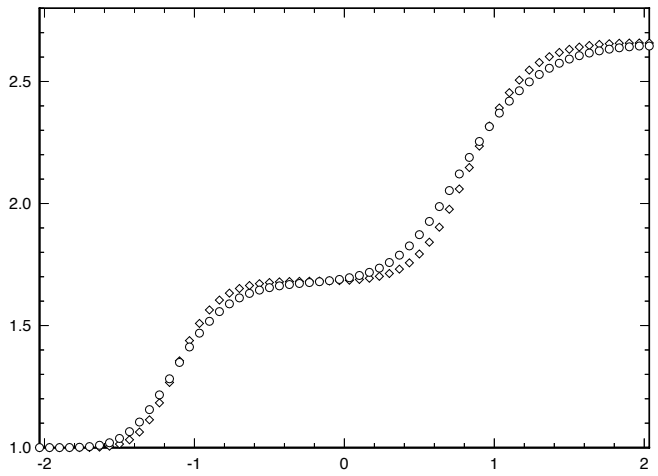

Figure 14: *Comparison of density profile for reflection problem along line $y = 0.525$: $\diamond$–MoT, $\circ$–VL.*

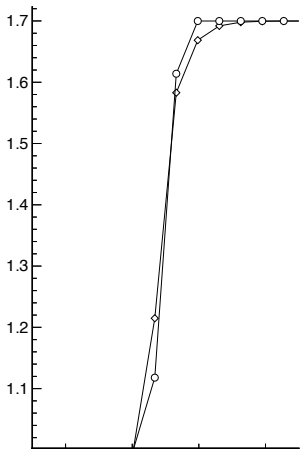

Figure 15: *1-D density profile for normal shock*

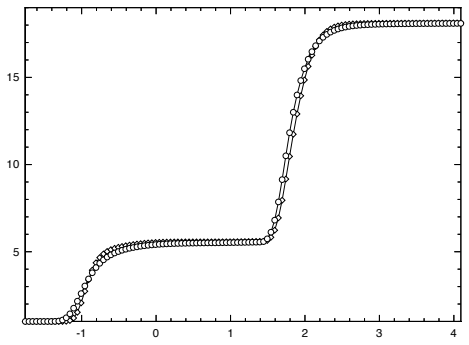

Figure 16: *Density profile for Mach 10 reflection problem along line $y = 0.525$: $\diamond$–MoT, $\circ$–VL.*

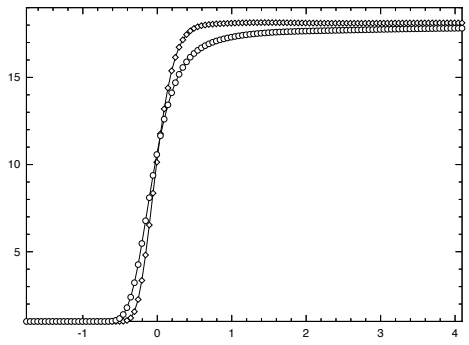

Figure 17: *Density profile for Mach 10 reflection problem along line $y = 0.0$: $\diamond$–MoT, $\circ$–VL.*

6 Conclusions

The aim of this paper is, to introduce a new approach towards the discretisation of the multi-dimensional Euler-equations. It is obvious, that the investigations shown are far from complete. The implemented scheme shows very robust behavior even for high Mach number flows. The method is also capable of capturing multidimensional effects.

Most of the drawbacks at hand of this method, i.e. the large complexity of the scheme and the first order approximation, can be overcome. A more general definition of the waves leads to a class of very efficient and simple multi-dimensional methods [10]. The correct interpretation of these schemes result in a linearization of the Euler-equations in several space dimensions [7]. It can also be shown, that there is no theoretical limit on the order of accuracy in smooth regions.

The extensive use of the homogeneity of the equation questions the generalization for other systems of conservation laws. As shown by A.-T. Morel in [17], it is possible to adapt this idea to the shallow water equation, a hyperbolic conservation law with inhomogeneous flux [5]. An adaption is also possible for the equations of magneto hydrodynamics [9].

Acknowledgment

Most of this work was done at ETH-Zürich and I would like to thank my former colleagues Rolf Jeltsch, Achim Schroll and Carsten Schulz-Rinne for lots of helpful discussions. I also want to thank Herb Keller and Stefan Vandervalle for their helpfull suggestions.

References

[1] Gabi Ben-Dor. *Shock Wave Reflection Phenomena*. Springer, 1992.

[2] Helmut Boeing. *Die numerische Konstruktion der exakten Lösung des skalaren Riemannproblems in zwei Raumdimensionen*. PhD thesis, RWTH Aachen, 1992.

[3] P. N. Childs and K. W. Morton. Characteristic galerkin methods for scalar conservation laws in one dimesion. *SIAM J. Numer. Anal.*, 27(3):533–594, 1990.

[4] Philip Collela. Multidimensional upwind methods for hyperbolic conservation laws. *J. of Comp. Phys.*, 87:171–200, 1990.

[5] M. Fey, R. Jeltsch, and A.-T. Morel. Multidimensional schemes for nonlinear systems of hyperbolic conservation laws. Technical Report 95-11, Seminar für Angewandte Mathematik, ETH Zürich, 1995. to appear in "Proceedings of the 16th Biannual Conference on Numerical Analysis", University of Dundee, June 27-30, 1995, Ed. D. Griffiths, 1996.

[6] Michael Fey. *Ein echt mehrdimensionales Verfahren zur Lösung der Eulergleichungen*. PhD thesis, ETH Zürich, 1993.

[7] Michael Fey. Decomposition of the multidimensional euler equations into advection equations. Technical Report 95-14, Seminar für Angewandte Mathematik, ETH Zürich, 1995.

[8] Michael Fey. Approximation and stability analysis for the high order method of transport for the linear advection problem. Technical report, Seminar für Angewandte Mathematik, ETH Zürich, in preparation.

[9] Michael Fey. The method of transport for the multi-dimensional equations of magneto hydrodynamic. Technical report, Seminar für Angewandte Mathematik, ETH Zürich, in preparation.

[10] Michael Fey and Rolf Jeltsch. A simple multidimensional Euler scheme. In Ch. Hirsch, editor, *Proceedings of the First European Computational Fluid Dynamics Conference, Brussels, 7-11 September 1992*. Elsevier Science Publishers, 1992.

[11] Michael Fey and Achim Schroll. Monoton split- and unsplit methods for a single conservation law in two space dimensions. Technical Report 57, Inst. für Geometrie und Praktische Mathematik, RWTH Aachen, 1989.

[12] S. K. Godunow. Die Differenzenmethode zur numerischen Berechnung von Unstetigkeitslösungen hydrodynamischer Gleichungen. *Mat. Sb.*, 47, 1959. deutsche Übersetzung.

[13] Ch. Hirsch, C. Lacor, and H. Deconinck. Convection algorithms based on a diagonalization procedure for the multidimensional Euler equations. In *AIAA 8th Computational Fluid Dynamics Conference*. AIAA, 1987.

[14] W. N. G. Hitchon, D.J. Koch, and J. B. Adams. An efficient scheme for convection-dominated transport. *J. of Comp. Rhys.*, 83:79–95, 1989.

[15] R. J. LeVeque. Simplified multidimensional flux limiter methods. In M.J. Baines and K. W. Morton, editors, *Numerical Methods for Fluid Dynamics*, volume 4. Oxford University Press, 1993.

[16] Randall J. LeVeque. High resolution finit volume methods on arbitrary grids via wave propagation. *J. Comp. Phys.*, 78(1):36–63, 1988.

[17] A.-T. Morel. Multidimensional method of transport for the shallow water equation. Presentation at 5-th Intern. Conf. on Hyperbolic Problems, Stony Brook, NY, June 13-17 1994.

[18] H. Paillere, H. Deconick, R. Struijs, P. Roe, L. Mesaros, and J. Müller. Technical report, AIAA Report No. 93-3301 CP, 1993.

[19] P. L. Roe. Beyond the Riemann Problem. *ICASE-NASA*. Langley workshop, September 1991.

[20] P. L. Roe. Approximate Riemann solvers, parameter vectors, and difference schemes. *J. Comp. Physics*, 43:357–372, 1981.

[21] P. L. Roe. Linear advection schemes on triangular meshes. Technical Report CoA Rep. No. 8720, Cranfield, 1987.

[22] P.L. Roe. A basis for upwind differencing of the two-dimensional unsteady Euler equation. In K.W. Morton and M.J. Baines, editors, *Numerical Methods for Fluid Dynamics II*, pages 59–80. Oxford, 1986.

[23] P.L. Roe, R. Struijs, and H. Deconinck. A conservative linearisation of the multidimensional euler equations. 1991.

[24] Carsten W. Schulz-Rinne, James P. Collins, and Harland M. Glaz. *Numerical Solution of the Riemann Problem for Two-Dimensional Gas Dynamics*. Research Report No. 92-02, Seminar für Angewandte Mathematik, ETH Zürich, 1992.

[25] J. Smoller. *Shock Waves and Reaction–Diffusion Equations*. Springer Verlag, 1983.

[26] J. L. Steger and R. F. Warming. Flux vector splitting of the inviscid gasdynamic equations with application to finite difference methods. *J. Comp. Phys.*, 40(263-293), 1981.

Research Reports

No.	Authors	Title
95-15	M. Fey	The Method of Transport for solving the Euler-equations
95-14	M. Fey	Decomposition of the multidimensional Euler equations into advection equations
95-13	M.D. Buhmann	Radial Functions on Compact Support
95-12	R. Jeltsch	Stability of time discretization, Hurwitz determinants and order stars
95-11	M. Fey, R. Jeltsch, A.-T. Morel	Multidimensional schemes for nonlinear systems of hyperbolic conservation laws
95-10	T. von Petersdorff, C. Schwab	Boundary Element Methods with Wavelets and Mesh Refinement
95-09	R. Sperb	Some complementary estimates in the Dead Core problem
95-08	T. von Petersdorff, C. Schwab	Fully discrete multiscale Galerkin BEM
95-07	R. Bodenmann	Summation by parts formula for noncentered finite differences
95-06	M.D. Buhmann	Neue und alte These über Wavelets
95-05	M. Fey, A.-T. Morel	Multidimensional method of transport for the shallow water equations
95-04	R. Bodenmann, H.J. Schroll	Compact difference methods applied to initial-boundary value problems for mixed systems
95-03	K. Nipp, D. Stoffer	Invariant manifolds and global error estimates of numerical integration schemes applied to stiff systems of singular perturbation type - Part II: Linear multistep methods
95-02	M.D. Buhmann, F. Derrien, A. Le Méhauté	Spectral Properties and Knot Removal for Interpolation by Pure Radial Sums
95-01	R. Jeltsch, R. Renaut, J.H. Smit	An Accuracy Barrier for Stable Three-Time-Level Difference Schemes for Hyperbolic Equations
94-13	J. Waldvogel	Circuits in Power Electronics
94-12	A. Williams, K. Burrage	A parallel implementation of a deflation algorithm for systems of linear equations
94-11	N. Botta, R. Jeltsch	A numerical method for unsteady flows
94-10	M. Rezny	Parallel Implementation of ADVISE on the Intel Paragon